

Quadruple-peaked spectral line profiles as a tool to constrain gravitational potential of shell galaxies

I. Ebrov^{1,2}, L. Jlkov^{3,4}, B. Jungwiert¹, M. Křzek^{1,5}, M. Blek^{1,2}, K. Bartořkov^{1,3}, T. Skalick³, and I. Stoklasov¹

¹ Astronomical Institute, Academy of Sciences of the Czech Republic, Bon II 1401/1a, CZ-141 31 Prague, Czech Republic
e-mail: ivana@ig.cas.cz

² Faculty of Mathematics and Physics, Charles University in Prague, Ke Karlovu 3, CZ-121 16 Prague, Czech Republic

³ Department of Theoretical Physics and Astrophysics, Faculty of Science, Masaryk University, Kotlřsk 2, CZ-611 37 Brno, Czech Republic

⁴ ESO, Alonso de Cordova 3107, Casilla 19001, Santiago, Chile

⁵ Astronomical Institute, Faculty of Mathematics and Physics, Charles University in Prague, V Holeřovikch 2, CZ-180 00 Prague, Czech Republic

Received ...; accepted ...

ABSTRACT

Context. Stellar shells observed in many giant elliptical and lenticular as well as a few spiral and dwarf galaxies, presumably result from galaxy mergers. Line-of-sight velocity distributions of the shells could, in principle, if measured with a sufficiently high S/N, constitute one of methods to constrain the gravitational potential of the host galaxy.

Aims. Merrifield & Kuijken (1998) predicted a double-peaked line profile for stationary shells resulting from a nearly radial minor merger. In this paper, we aim at extending their analysis to a more realistic case of expanding shells, inherent to the merging process, in the same type of merger and the same orbital geometry.

Methods. We use analytical approach as well as test particle simulations to predict the line-of-sight velocity profile across the shell structure. Simulated line profiles are convolved with spectral PSFs to estimate the peak detectability.

Results. The resulting line-of-sight velocity distributions are more complex than previously predicted due to non-zero phase velocity of the shells. In principle, each of the Merrifield & Kuijken (1998) peaks splits into two, giving a quadruple-peaked line profile, which allows more precise determination of the potential of the host galaxy and, moreover, contains additional information. We find simple analytical expressions that connect the positions of the four peaks of the line profile and the mass distribution of the galaxy, namely the circular velocity at the given shell radius and the propagation velocity of the shell. The analytical expressions were applied to a test-particle simulation of a radial minor merger and the potential of the simulated host galaxy was successfully recovered. The shell kinematics can thus become an independent tool to determine the content and distribution of the dark matter in shell galaxies, up to ~100 kpc from the center of the host galaxy.

Key words. Galaxies: kinematics and dynamics – Galaxies: halos – Methods: analytical – Methods: numerical – Galaxies: elliptical and lenticular, cD – Galaxies: interactions

1. Introduction

Several different methods have been used to measure the gravitational potentials and their gradients of elliptical galaxies, including strong and weak gravitational lensing (e.g., Gavazzi et al. 2007; Mandelbaum et al. 2008; Auger et al. 2010), X-ray observations of hot gas in the massive gas-rich galaxies (e.g., Fukazawa et al. 2006; Nagino & Matsushita 2009; Churazov et al. 2008; Das et al. 2010), rotation curves of detected disks and rings of neutral hydrogen (e.g., Weijmans et al. 2008), stellar-dynamical modelling from integrated light spectra (e.g., Weijmans et al. 2009; de Lorenzi et al. 2009; Churazov et al. 2010; Thomas et al. 2011), as well as using tracers such as planetary nebulae, globular clusters and satellite galaxies (e.g., Coccato et al. 2009; Nierenberg et al. 2011; Deason et al. 2012; Norris et al. 2012). All the methods have their limits, such as the redshift of the observed object, the luminosity profile, and gas content. In particular, the use of stellar dynamical modelling is plausible in the wide range of galactic masses, as long as spectroscopic data are available. However, it becomes more challenging beyond a few optical half-light radii. Other complementary gravitational tracers or techniques are required to derive mass

profiles in outer parts of the galaxies. When comparing independent techniques for the same objects at similar galactocentric radii, the discrepancies in the estimated circular velocity curves were revealed together with several interpretations (e.g., Churazov et al. 2010; Das et al. 2010). The compared techniques usually employ modelling the X-ray emission of the hot gas (assuming hydrostatic equilibrium) and dynamical modelling of the optical data in the massive early-type galaxies. Therefore, even for the most massive galaxies with X-ray observations available, there is a need for other methods to independently constrain the gravitational potential at various radii.

Shell galaxies are galaxies that contain arc-like fine features (first noticed by Arp 1966). These structures are made of stars and form open, (almost) concentric arcs which do not cross each other. Shells are relatively common in elliptical or lenticular galaxies. At least 10 % of all these galaxies in the local universe possess shells. Nevertheless, shells occur markedly most often in regions of low galaxy density and perhaps up to half of E and S0 galaxies in these environments are shell galaxies (Malin & Carter 1983; Schweizer 1983; Schweizer & Ford 1985; Colbert et al. 2001). Shells can be also associated with dust (Sikkema

et al. 2007; Stickel et al. 2004) and neutral hydrogen emission (Schiminovich et al. 1994, 1995; Balcells & Sancisi 1996; Petric et al. 1997; Horellou et al. 2001). In addition, Charmandaris et al. (2000) detected the presence of dense molecular gas in the shells of NGC 5128.

Shells are thought to be by-products of minor mergers of galaxies (Quinn 1984), although they can also be formed during major merger (Hernquist & Spergel 1992). The most regular shell systems are believed to result from nearly radial merger (Dupraz & Combes 1986; Hernquist & Quinn 1988). When a small galaxy enters the sphere of influence of a big elliptical galaxy on a radial or close-to-radial trajectory, it disintegrates and its stars begin to oscillate in the potential of the big galaxy. At their turning points, the stars have the lowest speed and thus tend to spend most of the time there – they pile up and produce arc-like structures in the luminosity profile of the host galaxy when viewed perpendicular to the axis of the collision.

Measurement of the number and distribution of shells can in principle lead to an approximate estimate of the mass distribution of the host galaxy and the time since the merger (Quinn 1984; Dupraz & Combes 1986; Hernquist & Quinn 1987a,b; Canalizo et al. 2007). But both of these observables are sensitive to details such as the dynamical friction and the gradual decay of the cannibalized galaxy during the merger (Dupraz & Combes 1987; James & Wilkinson 1987; Heisler & White 1990; Ebrov et al. 2010). Moreover, if the core of the cannibalized galaxy survives the merger, new generations of shells are added during each successive passage. This was predicted by Dupraz & Combes (1987) and successfully reproduced by Bartořkov et al. (2011) in self-consistent simulations. All these effects complicate the simulations to such an extent that the interest in shell galaxies largely faded by the end of the 80’s. Recently, this topic has raised interest again, thanks to the discovery of shells in a quasar host galaxy (Canalizo et al. 2007) and shell structures in M31 (Fardal et al. 2007, 2008) and in the Fornax dwarf (Coleman et al. 2004). Helmi et al. (2003) suggested that ring-like stellar structures, including the one observed in the outer disk of the Milky Way (so-called Monoceros ring), could be analogous to shells. A significant amount of shells is also contained in the early-type galaxy sample of the ongoing ATLAS^{3D} project, including images of galaxies with a surface brightness down to 29 mag/arcsec² (see e.g., Krajnovi et al. 2011; Duc et al. 2011). Kim et al. (2012) identified shells in about 6% of a sample of 65 early-type galaxies from the Spitzer Survey of Stellar Structure in Galaxies (S⁴G). Shells also appear to be suitable for indirect detection of dark matter via gamma-ray emission from dark matter self-annihilations (Sanderson et al. 2012). About 70 % of a complete sample of nearby (15–50 Mpc) luminous ($M_B < -20$ mag) elliptical galaxies were found to show tidal features by Tal et al. (2009). Faint structures, including shells and other signatures of recent gravitational interaction (tidal tails and streams), were found in the Sloan Digital Sky Survey (SDSS) – Kaviraj (2010) identified 18 % of early type galaxies (ETGs) in the SDSS Stripe82 sample to have disturbed morphologies; and similarly, Miskolczi et al. (2011) found tidal features in 19 % of their galaxies sample from SDSS DR7. Observations of warm gas by Rampazzo et al. (2003) in five shell galaxies showed irregular gaseous velocity fields (e.g., elongated gas distribution with asymmetric structure relative to the stellar body, or a double nucleus) and in most cases gas and stellar kinematics appear decoupled. Rampazzo et al. (2007), Marino et al. (2009), and Trinchieri et al. (2008) investigated star formation histories and hot gas content using the NUV and FUV GALEX (in the latter case also X-ray) observations in a few shell galax-

ies. The results support accretion events in the history of shell galaxies.

Merrifield & Kuijken (1998) (hereafter MK98) studied theoretically the kinematics of a stationary shell – a monoenergetic spherically symmetric system of stars oscillating on radial orbits in a spherically symmetric potential. They predict that spectral line profiles of such a system exhibit two clear maxima which provide a direct measure of the gradient of the gravitational potential at the shell radius. First attempt to analyze the kinematical imprint of a shell observationally was made by Romanowsky et al. (2012) using globular clusters as shell tracers in the early-type galaxy M87. Fardal et al. (2012) obtained radial velocities of giant stars in the so-called western shelf in M31 Andromeda galaxy. They successfully analyzed the shell pattern in the space of velocity versus radius.

Nevertheless, real-world shells are not stationary features: the stars of the satellite galaxy have a continuous energy distribution, and therefore the shell edge is, at different times, made of stars of different energies, as they continue to arrive at their respective turning points. Thus, the shell front appears to be traveling outwards from the center of the host galaxy and shell spectral line profiles are more complex (Jilkov et al. 2010, Ebrov et al. 2011, see also Fardal et al. 2012).

In this paper, we derive spectral-line profiles of non-stationary shells. We assume that shells originate from radial minor mergers of galaxies, as proposed by Quinn (1984). We find that both of the original MK98 peaks in the spectral line are split into two, resulting in a quadruple shape, which can still be used to constrain the host galaxy potential, and even bring additional information. We outline the simplified theoretical model and derive the shell velocities in Sect. 2, and describe the origin of the quadruple line profile in Sect. 3. In Sect. 4, we derive equations connecting the observable features of the quadruple-peaked LOSVD with parameters of the host galaxy potential in the vicinity of the shell edge. We compare these analytical predictions with the theoretical model (Sect. 5) and with results of test-particle simulations of the radial minor merger (Sect. 6). Section 6 also demonstrates the derivation of the galactic potential from the simulated spectral data.

2. Model of radial oscillations

If we approximate the shell system with a simplified model, we can describe its evolution completely depending only on the potential of the host galaxy. The approximation lies in the numerical integration of radial trajectories of stars in a spherically symmetric potential. The distribution of energies of stars is continuous, and these stars were released from a small volume in the phase space. We call it the model of radial oscillations and it corresponds to the notion that the cannibalized galaxy came along a radial path and disintegrated in the center of the host galaxy so that the stars were released at one moment in the center and began to oscillate freely on radial orbits. This approach was first used by Quinn (1984) followed by Dupraz & Combes (1986, 1987) and Hernquist & Quinn (1987a,b).

2.1. Turning points positions and their velocities

In shell galaxies, the shells are traditionally numbered using the serial number of the shell, n , from the outermost to the innermost (which in the model of radial oscillations for a single generation shell system corresponds to the oldest and the youngest shell, respectively). Imagine the cannibalized galaxy coming from the

right side of the host galaxy. Stars are released in the center of the host galaxy. Thereafter they reach their apocenters for the first time. But a shell does not form here yet, because the stars are not sufficiently phase wrapped. We call this the zeroth oscillation (the zeroth turning point) as we try to match the number of oscillations with the customary numbering scheme of the shells. We label the first shell that occurs on the right side (the same side from which the cannibalized galaxy approached) with $n = 1$. Shell no. 2 appears on the left side of the host galaxy, no. 3 on the right and so forth.

In the model of radial oscillations, the shells occur close to the radii where the stars are located in their apocenters at a given moment (the current turning point, r_{TP} , in our notation). The shell number n corresponds to the number of oscillations that the stars near the shell have completed or are about to complete. The current turning point r_{TP} must follow the equation

$$t = (n + 1/2)T(r_{\text{TP}}), \quad (1)$$

where t is the time elapsed since stars were released in the center of the host galaxy. $T(r)$ is the period of radial motion at a galactocentric radius r in the host galaxy potential $\phi(r)$:

$$T(r) = \sqrt{2} \int_0^r [\phi(r) - \phi(r')]^{-1/2} dr'. \quad (2)$$

The position of the current turning point evolves in time with a velocity given by the derivative of Eq. (1) with respect to radius

$$v_{\text{TP}}(r; n) = dr/dt = \frac{1}{dt/dr} = \frac{1}{n + 1/2} (dT(r)/dr)^{-1}. \quad (3)$$

We can clearly see from this relation (first derived by Quinn 1984) that any further turning point (turning point with higher n) at the same radius moves more slowly than the former one, causing a gradual densification of the space distribution of the shell system with time.

Technically, the reason for this densification is that the time difference between the moments when two stars with similar energy reach their turning points is cumulative. Let Δt be the difference in periods at two different radii r_a and r_b (imagine them on the right, $r_a < r_b$). The radius where stars complete the first oscillation moves from r_a to r_b in Δt . But in the second orbit on the left, the stars from r_b will already have a lag of Δt behind those from r_a and they are just getting a second one, so the third one (the second on the same side) reaches r_b from r_a in $2 \times \Delta t$. Every n -th completed oscillation on the right side then moves n times more slowly than the first one. The situation is similar on the left side and the shell system is getting denser. Moreover, the turning point has an additional lag of $1/2T(r_{\text{TP}})$, as the stars were released in the center of the host galaxy before their zeroth oscillation. This is the source of the factor $(n + 1/2)$ in Eqs. (1) and (2).

2.2. Real shells positions and velocities

Even in the framework of the radial oscillation model, it is not straightforward to express the position and velocity of the true edge of the shell. Photometrically, shells appear as brightening in the luminosity profile of the galaxy with a sharp cut-off. This is because the stars of the cannibalized galaxy occupy a limited volume in the phase space. With time, the shape of this volume gets thinner, more elongated and wrapped around invariant surfaces defined by the trajectories of the particles, increasing its coincidence with these surfaces. A shell appears close to the points where the invariant surface is perpendicular to the plane of

the sky (Nulsen 1989). For the n -th shell, it is the largest radius where stars about to complete their n -th oscillation are currently located. This radius is always larger than that of the current turning point of the stars that are completing their n -th oscillation. Thus the shell edge consists of outward moving stars about to complete their n -th oscillation.

Dupraz & Combes (1986) state that the stars forming the shell move with the phase velocity of the shell. We will show that this holds only approximately, yet we will use this equality in Sect. 4 to derive the relation between the shell kinematics and the potential of the host galaxy.

The position of a star, r_* , at a given time t since the release of the star in the center of the host galaxy is given by an implicit equation for r_* and it is a function of the star energy, or equivalently the position of its apocenter r_{ac} .¹ For stars having the integer part of $t/[2T(r_{\text{ac}})]$ odd, the equation reads:

$$t = (n + 1) \sqrt{2} \int_0^{r_{\text{ac}}} [\phi(r_{\text{ac}}) - \phi(r')]^{-1/2} dr' - \int_0^{r_*} [2(\phi(r_{\text{ac}}) - \phi(r'))]^{-1/2} dr', \quad (4)$$

and for stars that have completed an even number of half-periods (only such stars are found on the shell edge):

$$t = n \sqrt{2} \int_0^{r_{\text{ac}}} [\phi(r_{\text{ac}}) - \phi(r')]^{-1/2} dr' + \int_0^{r_*} [2(\phi(r_{\text{ac}}) - \phi(r'))]^{-1/2} dr'. \quad (5)$$

The first term in Eq. (5) corresponds to n radial periods for the star's energy (n is maximal so that $nT(r_{\text{ac}}) < t$), the other term corresponds to the time that it takes to reach radius r_* from the center of the galaxy. These equations are not analytically solvable even for the simplest galactic potentials and must be solved numerically.

The position of the n -th shell r_s equals to the maximal radius $r_{*,\text{max}}$, that solves Eq. (5) for the given n . The shell velocity v_s is obtained from the numerical derivative of a set of values of $r_{*,\text{max}}$ for several close values of t .

The stellar velocity at the shell edge is obtained by inserting $r_{*,\text{max}}$ with its corresponding r_{ac} into:

$$v(r_*) = \pm \sqrt{2[\phi(r_{\text{ac}}) - \phi(r_*)]}. \quad (6)$$

For the stars following Eq. (5), the velocity will be positive, for the rest negative.

It is clear that $v(r_{*,\text{max}}) \leq v_s$. Actually, $v(r_{*,\text{max}})$ is always slightly lower than the phase velocity of the shell, see Table 1. Meanwhile, the position of the shell for a given time is not far from the current turning point and their separation changes slowly. Thus the velocity of the turning points given in Eq. (3) is a good approximation for the shell velocity, see Fig. 3. Equation (3) is not generally solvable analytically either, but the numerical calculation of v_{TP} is much easier than determining the true velocity v_s as described in this chapter.

2.3. Shell stars kinematics

In the same model, we can also describe the line-of-sight velocity distribution (LOSVD) of a shell at a given time t , for a given potential of the host galaxy $\phi(r)$. In this paper, we model the host galaxy potential of the host galaxy as a double Plummer sphere as described in Sect. 6.1.

¹ As r_{ac} we denote the apocenter of the star corresponding to its energy, whereas r_{TP} (the current turning point) is the radius at which the stars reach their apocenters at the time of the measurement ("now").

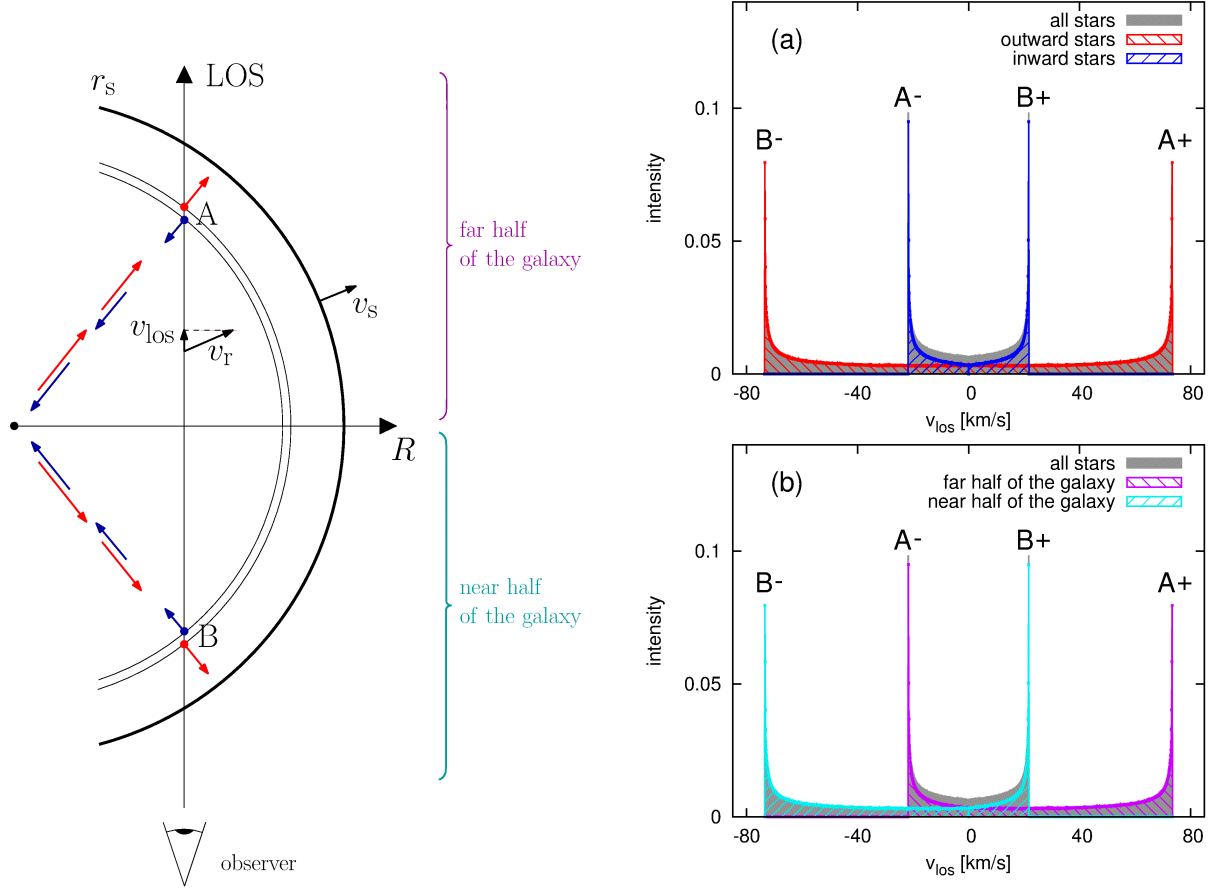


Fig. 1. Kinematics of a moving shell. Compare with Fig. 3 in MK98 for a stationary shell. Left: Scheme of the kinematics of a shell with radius r_s and phase velocity v_s . The shell is composed of stars on radial orbits with radial velocity v_r and line-of-sight velocity v_{los} . Right: The LOSVD at projected radius $R = 0.9r_s$, where $r_s = 120$ kpc (parameters of the shell are highlighted in bold in Table 1), in the framework of the model of radial oscillations (Sect. 2.3). The profile does not include stars of the host galaxy, which are not part of the shell system and are normalized so that the total flux equals one. (a) The LOSVD showing separate contributions from inward and outward stars; (b) the same profile, separated for contributions from the half of the host galaxy closer to the observer (the one including point B) and the more distant half (includes point A).

Eqs. (4) and (5) give the actual star position r_* and the shell number n for any apocenter r_{ac} in a range of energies. The radial velocity of a star on the particular radius is given by inserting the corresponding pair of r_{ac} and r_* in Eq. (6). Naturally, the projections of these velocities to the selected line-of-sight (LOS) form the LOSVD. To reconstruct the LOSVD, we have to add an assumption of the behavior of shell brightness in time. In Sect. 4.2, we show our choice of the behavior and we also show that the particular choice does not matter much.

3. Quadruple-peaked LOSVD

Fig. 1 illustrates a measurement of the LOSVD of stars in the shell, which is composed of inward and outward stars on radial trajectories. The stars near the edge of the shell move slowly. But it is clear from the geometry that contributions add up from different galactocentric distances, where the stars are either still traveling outwards to reach the shell, or already returning from their apocenters, to form a nontrivial LOSVD. MK98 showed that the maximal contribution to the LOSVD comes from stars at two particular locations along the line of sight (A and B), both of them at the same galactocentric distance.

In MK98’s stationary shell model, inward stars at the same radius differ from outward stars only in the sign of the line-of-

sight velocity v_{los} . This is not true when the edge of the shell moves outwards with velocity v_s . At any given instant, the stars that move inwards are returning from a point where the shell edge was at some earlier time, and so their apocenter is inside the current shell radius r_s . Similarly, the stars that move outwards will reach the shell edge in the future. Consequently, the stars that move inwards are always closer to their apocenter than those moving outwards at the same radius and thus their velocity is smaller. The inward stars move towards the observer in the farther of the two MK98 point (A), and away from us in the nearer point (B), while the stars moving outwards behave in the exactly opposite manner. Together, there are four possible velocities with the maximal contribution to the LOSVD, resulting in its symmetrical quadruple shape shown in Fig. 1. In fact, for a moving shell, points A and B are not at the same galactocentric radius for inward and outward stars. For inward stars, points A and B are a little closer to the center as indicated in Fig. 1. This is discussed in Sect. 4.3.

In the right-hand panel of Fig. 1, we used the model of radial oscillations as described in Sect. 2.3 to illustrate individual contributions to the LOSVD. MK98 constructed an analytical function describing the LOSVD close to the edge of their stationary shell model. This function exhibits intensity maxima that coincide with maximal/minimal velocity, leading to the symmetrical

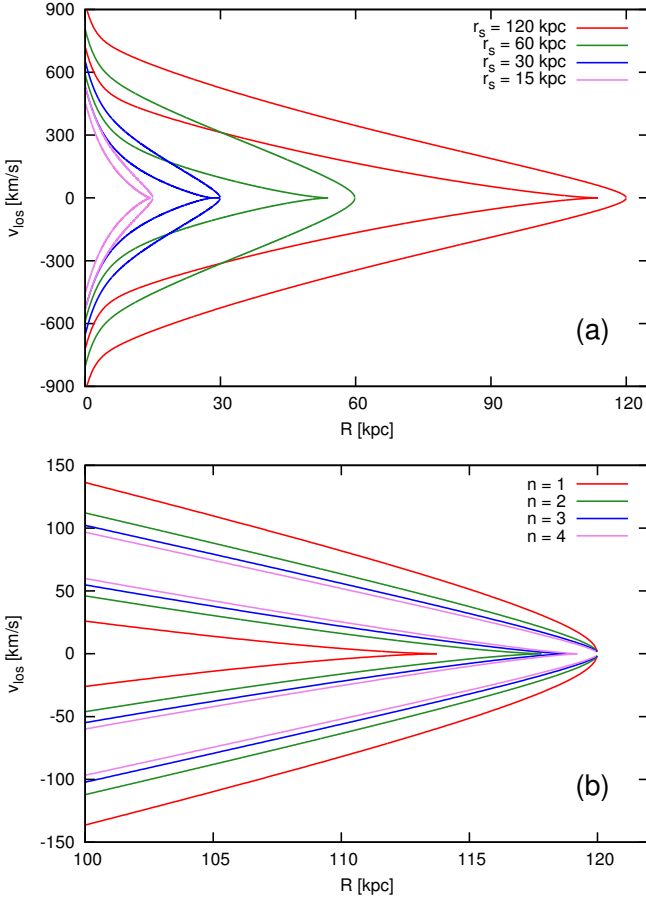


Fig. 2. Locations of peaks of the LOSVDs in the framework of the model of radial oscillations (Sect. 2.3): (a) for the first shell at different radii, (b) for the first up to the fourth shell at the radius of 120 kpc. The parameters of all shells are shown in Table 1. For parameters of the host galaxy potential see Sect. 6.1.

double-peaked profile with peaks at the edges of the LOSVD. This cannot be shown for a general moving shell, but Fig. 1 shows that the intensity maxima coincide with velocity extremes for separate contributions to the LOSVD.

The separation in velocity between peaks for a given projected radius R is given by the distance of R from the edge of the shell r_s . The profile shown in Fig. 1 corresponds to projected radius $R = 0.9r_s$. The closer to the shell edge, the narrower the profile is. The separation of the peaks at a given R depends on the phase velocity of the specific shell, near which we observe the LOSVD. This velocity is, for a fixed potential, given by the shell radius and its serial number (see Sect. 2.1). These effects are illustrated in Fig. 2, where we show the positions of the LOSVD peaks for the first shell at different radii r_s and for a shell at 120 kpc with different serial numbers n . Note that the higher the serial number n at a given radius, the smaller is the difference in the phase velocity between the two shells with consecutive serial numbers and thus in the positions of the respective peaks. Parameters of the corresponding shells can be found in Table 1.

The radial dependence of the phase velocity of the first four shells in the whole host galaxy is shown in Fig. 3. Using Eq. (3), we can see that the velocity of each subsequent shell differs from the first one only by the factor of $3/(1 + 2n)$. The rather large interval of the galactocentric radii where the shell velocity increases is caused by the presence of the halo with a large scaling parameter. In fact, we do not show the shell velocity, but the

Table 1. Parameters of shells for which the LOSVD intensity maxima are shown Fig. 2.

t Myr	n	r_s kpc	r_{TP} kpc	v_s km/s	$v(r_{s,max})$ km/s	v_{TP} km/s	v_c km/s
215	1	15	14.5	63.5	57.5	61.2	245
416	1	30	28.3	90.3	82.6	81.0	261
634	1	60	53.9	165.8	151.5	151.8	362
1006	1	120	113.9	142.4	133.3	141.8	450
1722	2	120	117.9	84.7	79.4	84.7	450
2428	3	120	118.9	60.3	54.6	60.3	450
3130	4	120	119.3	46.8	42.6	47.0	450

Notes. t : time since the release of stars at the center of the host galaxy, in which the shell has reached its current radius calculated in the framework of the model of radial oscillations (Sect. 2); n : serial number of shell (see Sect. 2.1); r_s : shell radius; v_s : shell phase velocity according to the method described in Sect. 2.2; r_{TP} : galactocentric radius of current turning points of the stars at this time given by Eq. (1); $v(r_{s,max})$: radial velocity of stars at the shell edge; v_{TP} : phase velocity of current turning point according Eq. (3); v_c : circular velocity at the shell edge radius. For parameters of the host galaxy see Sect. 6.1. The shell that is used in further Figs. 4, 6, 7, and 8 is highlighted in bold.

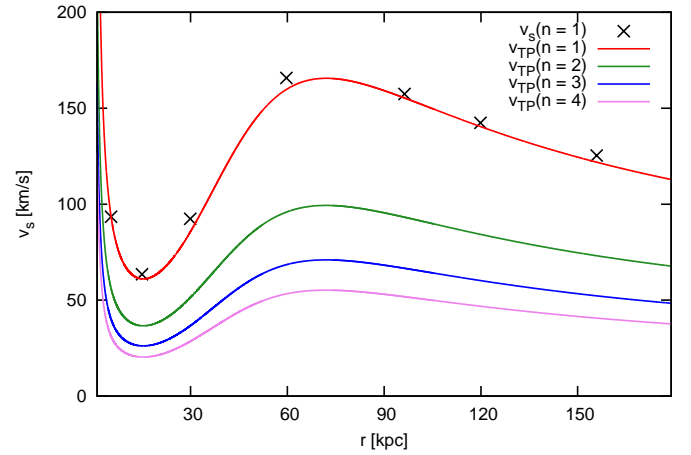


Fig. 3. Dependence of the phase velocity of the turning points on the galactocentric radius for the first four shells according to Eq. (3). For parameters of the host galaxy potential see Sect. 6.1. Black crosses show the true velocity of the first shell calculated for several radii according to the method described in Sect. 2.2. Keep in mind that in fact, the turning point responsible for the current location of shell is not at the same radius as the shell edge at the same time, but the difference is small (see Table 1).

velocity of the turning points at the same radius. Nevertheless, these are sufficiently close. Black crosses show the true velocity of the first shell calculated for several radii according to the method described in Sect. 2.2. For shells of higher n these differences between the phase velocity of a shell and the corresponding turning point with consecutive serial numbers are even smaller.

The radius of a stationary shell is the same as the radius of the apocenter of stars (as they all have the same energy), while the edge of a moving shell is at the radius which is always slightly further from the center than the current turning points. This difference creates an intricate zone between the radius of the current turning points and the radius of the edge where all the stars of a given shell move outwards. When the line-of-sight radius approaches (from lower radii) the turning points of the stars, the inner maxima of the LOSVD approach each other until

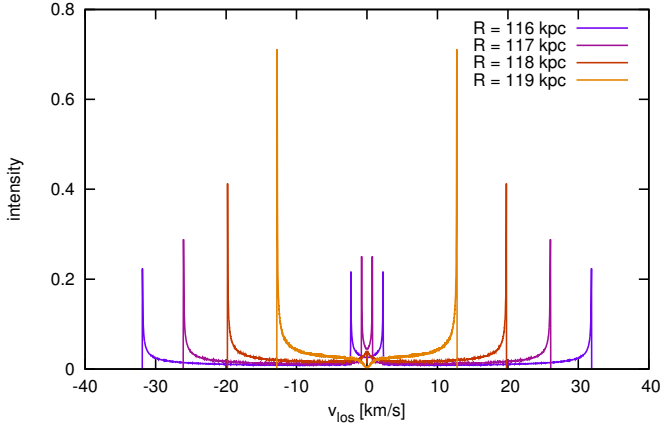


Fig. 4. Evolution of the LOSVD near the shell edge for the second shell at $r_s = 120$ kpc (parameters of the shell are highlighted in bold in Table 1) for the projected radius 116, 117, 118, and 119 kpc in the framework of the model of radial oscillations (Sect. 2.3). In this model, the current turning points of the shell particles are at $r_{TP} = 117.9$ kpc. Beyond this radius, the inner maxima disappear. Profiles do not include stars of the host galaxy, which are not part of the shell system and are normalized so that the total flux equals one. For parameters of the host galaxy potential see Sect. 6.1.

they merger and finally disappear, see Fig. 4. Closer to the shell edge than the current turning points, we will actually see a minimum in the middle of the LOSVD. The intricate zone is much larger for the first shell (for the shell radius of 120 kpc in our host galaxy potential it occupies 6 kpc for the first shell, 2 kpc for the second one, and less than one kpc for the fourth shell, see Table 1).

4. Relating observables to circular and shell velocities

The non-zero velocity of the shell complicates the kinematics of shells in two aspects already mentioned above. Due to the energy difference between inward and outward particles (at the same radius) the LOSVD peak is split into two, and the shell edge is not at the radius of the current turning point, but slightly further from the center of the host galaxy. In this section, we describe the LOSVD of such a shell in the approximation of a locally constant galactic acceleration and shell velocity. In addition, we assume that the velocity of stars at the edge of the shell is equal to the phase velocity of the shell.

4.1. Motion of a star in a shell system

The galactocentric radius of the shell edge is a function of time, $r_s(t)$. Let $t = 0$ be the moment of measurement and the position of the shell edge at this time be $r_s(0) = r_{s0}$. We assume the following: that the stars are on strictly radial orbits, that there is a locally constant value of the radial acceleration a_0 in the host galaxy potential and a locally constant velocity of the shell edge v_s , and that the stars at the shell edge have the same velocity as the shell. For each star, its galactocentric radius at any time is $r(t)$, while t_s is the time when the star could be found at the shell edge $r_s(t_s)$. Then the equation of motion and the initial conditions for the star near a given shell radius are:

$$\frac{d^2 r(t)}{dt^2} = a_0, \quad (7)$$

$$\left. \frac{dr(t)}{dt} \right|_{t=t_s} = v_s, \quad (8)$$

$$r(t_s) = r_s(t_s) = v_s t_s + r_{s0}. \quad (9)$$

The solution of these equations is

$$r(t) = a_0(t - t_s)^2/2 + v_s(t - t_s) + r_s(t_s), \quad (10)$$

$$v(t) = v_s + a_0(t - t_s), \quad (11)$$

and the actual position of the star $r(0)$ and its radial velocity $v(0)$ at time of measuring ($t = 0$) are

$$r(0) = t_s^2 a_0/2 + r_{s0}, \quad (12)$$

$$v(0) = v_s - a_0 t_s. \quad (13)$$

Eliminating t_s from the two previous equations, we get

$$v(0)_{\pm} = v_s \pm v_c \sqrt{2(1 - r(0)/r_{s0})}, \quad (14)$$

where $v_c = \sqrt{-a_0 r_{s0}}$ is the circular velocity at the shell edge radius.

4.2. Approximative LOSVD

The projection of the velocity given by Eq. (14) to the line-of-sight at a projected radius R will be

$$\begin{aligned} v_{los\pm} &= \sqrt{1 - R^2/(r(0))^2} v(0)_{\pm} = \\ &= \sqrt{1 - R^2/(r(0))^2} \left[v_s \pm v_c \sqrt{2(1 - r(0)/r_{s0})} \right]. \end{aligned} \quad (15)$$

Using this expression, we can model the LOSVD at a given projected radius for a given shell. For the proper choice of a pair of values v_c and v_s we can find a match with observed and modeled peaks of the LOSVD.

To model the LOSVD in both frameworks – the model of radial oscillations (Sect. 2.3) and the approximative LOSVD by Eq. (15), we have to add an assumption of the behavior of the shell brightness in time or in space (as the shell expands with time). This behavior depends on the parameters of the merger that has produced the shells. It is determined by the energy distribution of stars of the cannibalized galaxy in the instant of its decay in the center of the host galaxy. For simplicity, we choose the density at the surface of a sphere of shell edge radius r_s to be $\Sigma_{sph}(r_s(t)) \sim 1/r_s^2(t)$, corresponding to a shell containing the same number of stars at each moment. The relation between $\Sigma_{sph}(r_s(t))$ and the projected surface density near the shell edge on the sky $\Sigma_{los}(r_s(t))$ is $\Sigma_{los}(r_s(t)) \sim \sqrt{r_s(t)} \Sigma_{sph}(r_s(t))$. It turns out that no reasonable choice of this function has an effect on the general characteristics of the LOSVD and the principles of its formation that we describe in this paper. For illustration, we show the LOSVD of Σ_{sph} increasing as r^2 and Σ_{sph} decreasing as $1/r^2$ in Fig. 5. For the profiles shown, the ratio of the inner and outer peaks changes with the change of the Σ_{sph} , but the peak positions are unaffected and the overall shape of the profile does not alter significantly. For the shells that were created in a radial minor merger, we can expect a sharp rise of the shell brightness near the center of the host galaxy followed by an extensive area of its decrease. The fact that the main features of the LOSVD do not depend on the choice of Σ_{sph} means that our method to measure the potential of shell galaxies is not sensitive in this respect to the details of the decay of the cannibalized galaxy.

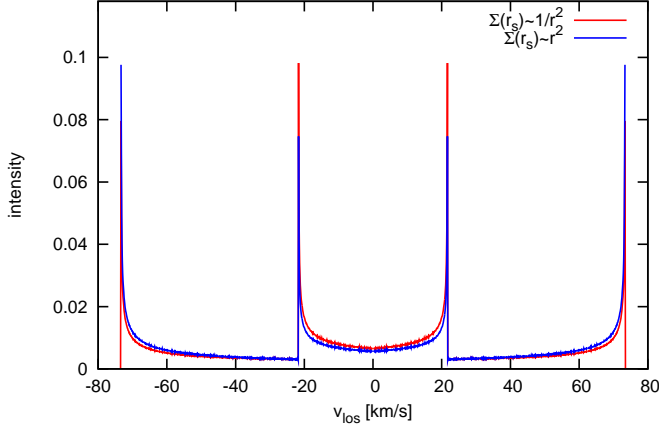


Fig. 5. LOSVD of the second shell at $r_s = 120$ kpc (parameters of the shell are highlighted in bold in Table 1) for the projected radius 108 kpc in the framework of the model of radial oscillations (Sect. 2.3), where the density at the surface of a sphere of shell edge radius r_s is $\Sigma_{\text{sph}}(r_s(t)) \sim r_s^2(t)$ for the blue curve and $\Sigma_{\text{sph}}(r_s(t)) \sim 1/r_s^2(t)$ for the red one. The profile does not include stars of the host galaxy, which are not part of the shell system and are normalized so that the total flux equals one.

4.3. Radius of maximal LOS velocity

MK98 proved that 1) near the edge of a stationary shell, r_s , the maximum intensity of the LOSVD is at the point where the maximal absolute value of the line-of-sight velocity are located; 2) the maximal absolute value of the line-of-sight velocity $v_{\text{los,max}}$ comes from stars at the galactocentric radius

$$r_{\text{vmax}} = \frac{1}{2}(R + r_{s0}), \quad (16)$$

at each projected radius R .

For a moving shell, analogous equations are significantly more complex and a similar relation cannot be easily proven, but we apply both results of MK98 and we show on examples (Figs. 7, 8, 11, and 12) that their use is valid even for non-stationary shells. In the framework of the radial oscillations model (Sect. 2.3), we have already shown that the peaks of the LOSVD occur fairly close to the edges of distributions of inward and outward stars (see Fig. 1 right). The peaks are also near the edges of the LOSVD, if we divide the LOSVD into the contributions of the near and the far half of the galaxy as in Fig. 1 (b). The inner peak corresponds to inward moving stars and the outer one to the outward moving ones. This approach is used in the following equations (Sect. 4.4). The maximal line-of-sight velocity corresponds to the outer peak and the minimal to the inner one. Reasons and justification for usage of Eq. (16) for r_{vmax} is discussed in Sect. 5, point 3 (see also Fig. 6).

4.4. Approximative maximal LOS velocity

Using the results of MK98, we derive an expression for the maxima/minima of the line-of-sight velocity (corresponding to locations of the LOSVD peaks) in observable quantities (namely the maxima/minima of the LOS velocity, the projected radius, and the shell radius) by substituting r_{vmax} given by Eq. (16) for $r(0)$ in Eq. (15)

$$v_{\text{los,max}\pm} = \left(v_s \pm v_c \sqrt{1 - R/r_{s0}} \right) \times \sqrt{1 - 4(R/r_{s0})^2 (1 + R/r_{s0})^{-2}}. \quad (17)$$

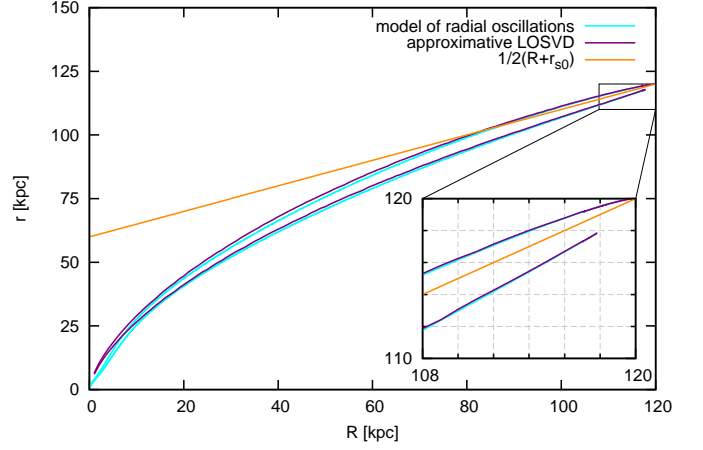


Fig. 6. Galactocentric radii r_{vmax} , that contribute to the LOSVD at the maximal velocities according to Eq. (16) (which was used in the derivation of the approximative maximal/minimal LOS velocities (see Sect. 5, point 3)) – orange curve, according to the approximative LOSVD (see Sect. 5, point 2) – purple curves, and according to the model of radial oscillations (Sect. 2.3) – light blue curves for the second shell at 120 kpc (parameters of the shell are highlighted in bold in Table 1). For parameters of the host galaxy potential see Sect. 6.1.

For the measured locations of the LOSVD peaks $v_{\text{los,max+}}$, $v_{\text{los,max-}}$, projected radius R , and shell edge radius r_{s0} , we can express the circular velocity v_c at the shell edge radius and the current shell velocity v_s using inverse equations:

$$v_c = \frac{|v_{\text{los,max+}} - v_{\text{los,max-}}|}{2\sqrt{(1 - R/r_{s0})[1 - 4(R/r_{s0})^2(1 + R/r_{s0})^{-2}]}} \quad (18)$$

$$v_s = \frac{v_{\text{los,max+}} + v_{\text{los,max-}}}{2\sqrt{1 - 4(R/r_{s0})^2(1 + R/r_{s0})^{-2}}}. \quad (19)$$

Alternatively, the value of the circular velocity v_c at the shell edge radius could be inferred from measurements of positions of peaks at two or more different projected radii for the same shell: let $\Delta v_{\text{los}} = v_{\text{los,max+}} - v_{\text{los,max-}}$, where $v_{\text{los,max}\pm}$ satisfy Eq. (17). Then, in the vicinity of the shell edge,

$$\Delta v_{\text{los}} = 2v_c \sqrt{(R/r_{s0} - 1)[1 - 4(R/r_{s0})^2(1 + R/r_{s0})^{-2}]} \approx 2(1 - R/r_{s0})v_c, \quad (20)$$

and taking the derivative with respect to the projected radius

$$\frac{d \Delta v_{\text{los}}}{dR} = -2 \frac{v_c}{r_{s0}}, \quad (21)$$

which happens to be the same expression as equation (7) in MK98. Nevertheless, in MK98, Δv_{los} is the distance between the two LOSVD intensity maxima of a stationary shell, whereas in our framework it is the distance between the outer peak for positive velocities and the inner peak for negative velocities or vice versa. This equation allows us to measure the circular velocity in shell galaxies using the slope of the LOSVD intensity maxima in the $R - v_{\text{los}}$ diagram.

5. Comparison of models

In this section, we compare three different approaches to the theoretical calculation of the maximal/minimal line-of-sight velocities (which are equivalent to the positions of LOSVD peaks):

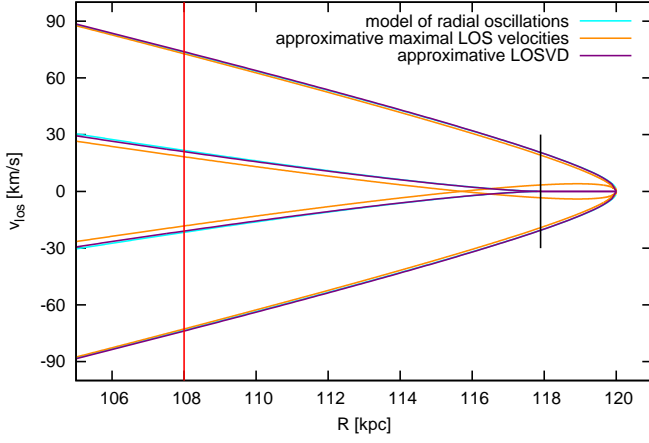


Fig. 7. LOSVD peak locations for the second shell at the radius of 120 kpc (parameters of the shell are highlighted in bold in Table 1) according to the approximative maximal LOS velocities (see Sect. 5, point 3)–Eq. (17) (orange curves); the approximative LOSVD (see Sect. 5, point 2)–Eq. (15) (purple curves); and the model of radial oscillations (Sect. 2.3) (light blue curves almost merged with the purple one). The red line shows the position of the LOSVD from Fig. 8, the black one shows the position of the current turning points. For parameters of the host galaxy potential see Sect. 6.1.

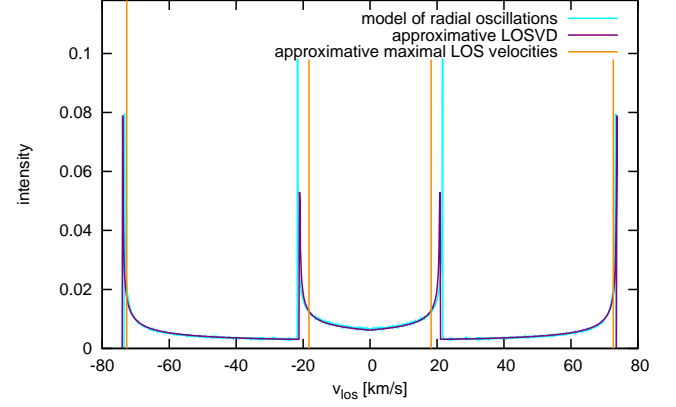


Fig. 8. LOSVD of the second shell at $r_s = 120$ kpc (parameters of the shell are highlighted in bold in Table 1) for the projected radius $R = 0.9r_s = 108$ kpc according to the approximative LOSVD (see Sect. 5, point 2)–Eq. (15) (purple curve) and the model of radial oscillations (Sect. 2.3) (light blue curve almost merged with the purple one). Locations of peaks as given by the approximative maximal LOS velocities (see Sect. 5, point 3)–Eq. (17) are plotted with orange lines. Profiles do not include stars of the host galaxy that are not part of the shell system and are normalized so that the total flux equals to one. For parameters of the host galaxy potential see Sect. 6.1.

1. Using the model of radial oscillations as described in Sect. 2.3 (these results are plotted with light blue curves in relevant figures): this model requires a complete knowledge of the potential of the host galaxy, obviously unavailable for real galaxies.
2. Using the approximative LOSVD (purple curves): For the given shell at the chosen projected radius, Eq. (15) is a function of only two parameters: the circular velocity v_c at the shell edge radius and the current shell velocity v_s . With the assumption of the behavior of the shell brightness as a function of the shell radius, Eq. (15) allows us to plot the whole LOSVD (see Sect. 4.2). However, the computation of the LOSVD and the peaks positions requires a numerical approach in this framework.
3. Using the approximative maximal LOS velocities (orange curves): Eq. (17) supplies directly the positions of the peaks. It differs from the previous approximation in the assumption about the galactocentric radius r_{vmax} from which the contribution to the LOSVD at the maximal speed comes. The assumption is that r_{vmax} is given by Eq. (16), which was derived by MK98 for a stationary shell. This equation is actually only very approximate, but allows us to analytically invert Eq. (17) to obtain formulae for the calculation of v_c and v_s from the measured peak positions in the spectrum of the shell galaxy near the shell edge (Eqs. (18) and (19)). For a moving shell, we could not derive any more accurate formula for r_{vmax} that would be simple enough to make the calculation of v_c and v_s feasible.

Fig. 6 shows a comparison of the radii that contribute to the LOSVD at the maximal velocities according to all three approaches. For the first two methods, the radius corresponding to the inner maxima of the LOSVD (which are the maxima created by the inward stars) is lower than that for the outer maxima, whereas Eq. (16) assumes the same r_{vmax} for both inward and outward stars.

Fig. 7 shows locations of the LOSVD peaks for the second shell at the radius of 120 kpc near the shell edge radius. The

purple curve is calculated using the approximative LOSVD (see Sect. 5, point 2)–Eq. (15), into which we inserted the velocity of the second shell according to the model of radial oscillations and the circular velocity in the potential of the host galaxy (see Sect. 6.1 for parameters of the potential). The purple curve does not differ significantly from the light blue curve calculated in the model of radial oscillations (see Sect. 2.3). The more important deviations in the orange curve of the approximative maximal LOS velocities (see Sect. 5, point 3)–Eq. (17) are due to using Eq. (16) for r_{vmax} . With this assumption, approximative maximal LOS velocities (the orange curve) predict that around the zone between the current turning point and the shell edge, the inner peaks change signs (this means that for the part of the galaxy closer to the observer, both inner and outer peaks will fall into negative values of the line-of-sight velocity and vice versa), whereas from the model of the radial oscillations we already know that the signal from the inner peak in a given (near or far) part of the galaxy is always either zero, or has the opposite sign to that of the outer peak.

The model of the radial oscillations and the approximative LOSVD–Eq. (15) were also used to construct the LOSVD for the second shell located at 120 kpc, at the projected radius of 108 kpc at Fig. 8. The graph also shows the locations of the peaks using the approximative maximal LOS velocities–Eq. (17).

6. Test-particle simulation of the merger

We performed a simplified simulation of formation of shells in a radial galactic minor merge. Both merging galaxies are represented by smooth potential. Millions of test particles were generated so that they follow the distribution function of the cannibalized galaxy at the beginning of the simulation. The particles then move according to the sum of the gravitational potentials of both galaxies. When the centers of the galaxies pass through each other, the potential of the cannibalized galaxy is suddenly switched off and the particles continue to move only in the fixed potential of the host galaxy. We use the simulation to demonstrate the validity of our methods of recovering the parameters

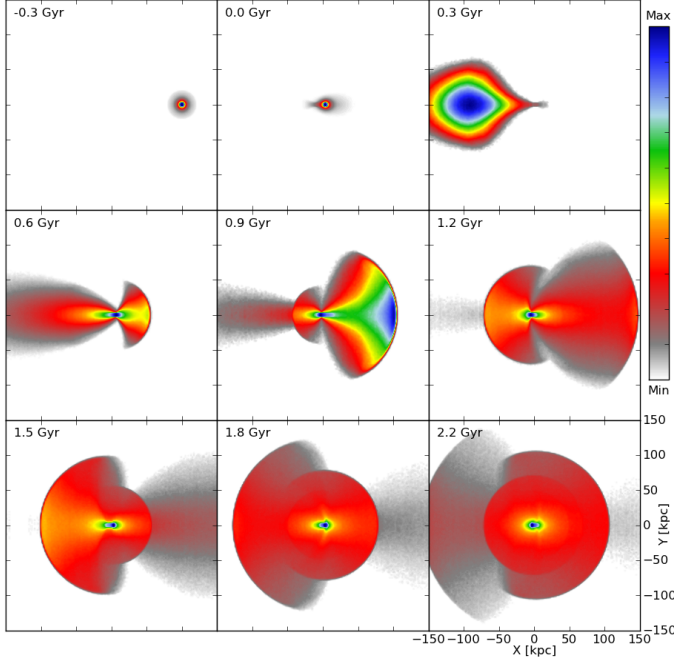


Fig. 9. Snapshots from our test-particle simulation of the radial minor merger, leading to the formation of shells. Each panel covers 300×300 kpc and is centered on the center of the host galaxy. Only the surface density of particles originally belonging to the satellite galaxy is displayed. The density scale varies between frames so that the respective range of densities is optimally covered.

of the host galaxy potential by “measuring” the positions of the peaks in the spectral lines. In all cases, we look at the galaxy from the view perpendicular to the axis of collision so that the cannibalized galaxy originally flew in from the right.

6.1. Parameters of the simulation

The potential of the host galaxy is modeled as a double Plummer sphere with respective masses $M_* = 2 \times 10^{11} M_\odot$ and $M_{DM} = 1.2 \times 10^{13} M_\odot$, and Plummer radii $b_* = 5$ kpc and $b_{DM} = 100$ kpc for the luminous component and the dark halo respectively. This model has properties consistent with observed massive early-type (and even shell) galaxies (Auger et al. 2010; Nagino & Matsushita 2009; Fukazawa et al. 2006). The potential of the cannibalized galaxy is chosen to be a single Plummer sphere with the total mass $M = 2 \times 10^{10} M_\odot$ and Plummer radius $b_* = 2$ kpc.

The cannibalized galaxy is released from rest at a distance of 100 kpc from the center of the host galaxy. When it reaches the center of the host galaxy in 306.4 Myr, its potential is switched off and its particles begin to oscillate freely in the host galaxy. The shells start appearing visibly from about 50 kpc of galactocentric distance and disappear at around 200 kpc, as there are very few particles with apocenters outside these radii, see Fig. 9.

6.2. Comparison of the simulation with models

In the simulations, some of the assumptions that we used earlier (Sect. 2) are not exactly fulfilled. Namely: 1) the particles do not move exactly radially, but on more general trajectories – which are, even in the case of a radial merger, nevertheless very eccentric; 2) all the particles are not released from the cannibalized galaxy right in the center of the host galaxy – when the potential

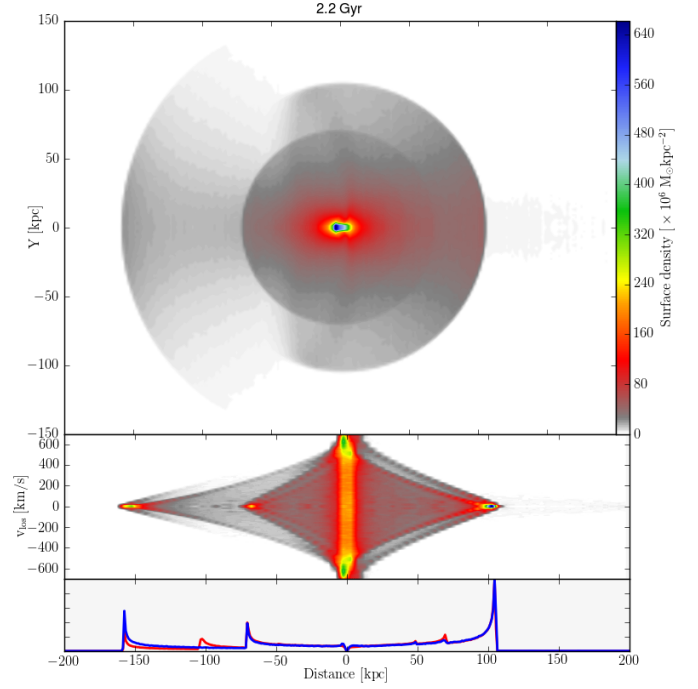


Fig. 10. Simulated shell structure 2.2 Gyr after the decay of the cannibalized galaxy. Only the particles originally belonging to the cannibalized galaxy are taken into account. Top: surface density map; middle: the LOSVD density map of particles in the ± 1 kpc band around the collision axis; bottom: histogram of galactocentric distances of particles. The angle between the radial position vector of the particle and the x -axis (the collision axis) is less than 90° for the blue curve and less than 45° for the red curve. The horizontal axis corresponds to the projected distance X in the upper panel, to the projected radius R in the middle panel and to the galactocentric distance r in the lower panel.

is switched off, the particles are located in the broad surroundings of the center and some are even released before the decay of the galaxy. These effects lead to a smearing of the kinematical imprint of shells, as the turning points are not at a sharply defined radius, but rather in some interval of radii for a given time.

The model of radial oscillations presented Sect. 2 predicts that 2.2 Gyr after the decay of the cannibalized galaxy (see Fig. 10) five outermost shells should lie at the radii of 257.3, -157.8 , 105.1, -70.5 , and 48.8 kpc. The negative radii refer to the shell being on the opposite side of the host galaxy with respect to the direction from which the cannibalized galaxy flew in. These radii are in a very good agreement with the radii of the shells “measured” in the simulation 2.2 Gyr after the decay of the cannibalized galaxy. In the simulation, the first shell (at 257.4 kpc) is composed of a few particles only, and therefore we will not consider it (its parameters in Table 2 are listed for completeness). Thus the outermost relevant shell in the system lies at -157.8 kpc and has a serial number $n = 2$. Also the shell at 48.8 kpc suffers from the lack of particles, but we will include it nevertheless.

Fig. 11 shows the comparison between the LOSVD in the simulation, the peaks of the LOSVD computed in the model of radial oscillations (light blue curves), and the approximative maximal LOS velocities – Eq. (17) (orange curves). To evaluate the approximative maximal LOS velocities, we have obtained the shell velocity $v_{s,model}$ from the model of radial oscillations (Sect. 2) for the respective serial number n of the shell and circu-

Table 2. Parameters of the shells in a simulation 2.2 Gyr after the decay of the cannibalized galaxy.

r_s kpc	n	$r_{TP,model}$ kpc	$v_{s,sim}$ km/s	$v_{s,model}$ km/s	$v_{c,model}$ km/s
48.8	5	48.5	38.7 ± 2.1	38.7	326
-70.6	4	-69.9	59.8 ± 1.6	54.3	390
105.0	3	103.9	68.1 ± 1.9	63.5	441
-157.8	2	-155.7	74.3 ± 1.2	72.4	450
257.4	1	251.0	97.5 ± 1.4	95.7	406

Notes. The values of $r_{TP,model}$ and $v_{s,model}$ are calculated for the shell position r_s and its corresponding serial number n according to the model of radial oscillations (see Sect. 2). The shell velocity $v_{s,sim}$ is derived from twenty positions between the times 2.49–2.51 Gyr for each shell. The value $v_{c,model}$ corresponds to the circular velocity at the shell edge radius r_s for the chosen potential of the host galaxy (see Sect. 6.1).

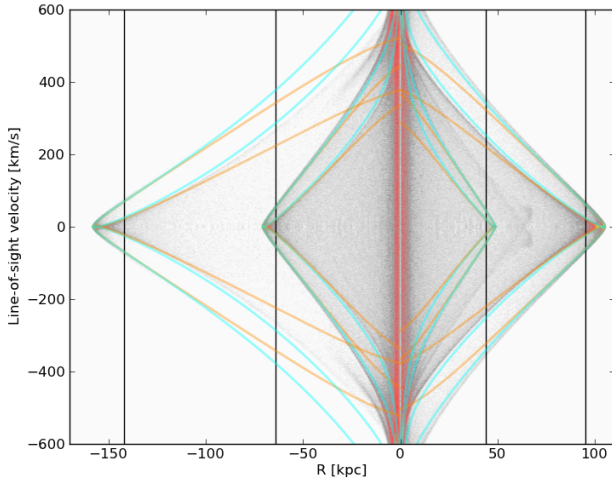


Fig. 11. LOSVD map of the simulated shell structure 2.2 Gyr after the decay of the cannibalized galaxy (middle panel in Fig. 10). Light blue curves show locations of the maxima according to the model of radial oscillations (Sect. 2.3) for shell radius r_s , corresponding serial number n , and for the known potential of the host galaxy (Sect. 6.1); orange curves are derived from the approximative maximal LOS velocities (see Sect. 5, point 3)–Eq. (17) for r_s , $v_{s,model}$, and $v_{c,model}$. Parameters of the shells are shown in Table 2. Black lines mark the location at $0.9r_s$ for each shell. The LOSVD for these locations are shown in Fig. 12. The map includes only stars originally belonging to the cannibalized galaxy.

lar velocity $v_{c,model}$ at the shell edge radius, using our knowledge of the potential of the host galaxy (see Sect. 6.1 for parameters of the potential). The values of all the respective shell quantities are listed in Table 2.

Fig. 11 also shows the locations that correspond to the radii of $0.9r_s$ for each individual shell (black lines). The LOSVD for these locations is shown in Fig. 12. The positions of simulated LOSVD peaks agree fairly well with all three theoretical approaches described in Sect. 5.

6.3. Recovering the potential from the simulated data

We have used a snapshot from our simulation, 2.2 Gyr after the decay of the cannibalized galaxy, as a source of the simulated data and we have tried to reconstruct the parameters of the potential of the host galaxy from the locations of the LOSVD peaks “measured” from the simulated data.

For a given host galaxy the signal-to-noise ratio in the simulated data is a function of the number of simulated particles, on the age of the shell system, on the distribution function of the cannibalized galaxy, and on its impact velocity. For a given radius in the simulated data, we can obtain arbitrarily good or bad signal-to-noise ratio by tuning these parameters. Thus we have adopted the universal criteria: 1) the LOSVD of each shell is observed down to 0.9 times its radius; 2) we “measured” the positions of the LOSVD peaks in different locations within the shell, sampled by 1 kpc steps. For the same reason, we do not estimate the errors, since in the real data will be dominated by other sources. We quote only the mean square deviation and the standard error of the linear regression.

These criteria give us between 7 and 15 “measurements” for a shell. Each “measurement” contains two values: the positions of the outer and inner peaks, $v_{los,max+}$ and $v_{los,max-}$ respectively, for each projected radius R (see green crosses in Fig. 13).

First we used the approximative maximal LOS velocities–Eqs. (18) and (19) for a direct calculation of the circular velocity $v_{c,eq(18)}$ at the shell edge radius r_s and the current shell velocity $v_{s,eq(19)}$. These equations are the inverse of Eq. (17), which corresponds to the model shown in orange lines in pictures throughout the text (see Sect. 5, point 3). Mean values from all the “measurements” for each shell are shown in Tables 3 and 4.

We obtain a better agreement with the circular velocity of our host galaxy potential when using the slope of the LOSVD intensity maxima–Eq. (21), where we fit the linear function of the “measured” distance between the outer and the inner peak on the projected radius, see $v_{c,slope}$ in Table 3 and in Fig. 14.

From the approximative maximal LOS velocities (see Sect. 5, point 3)–Eq. (17) we can derive a hybrid relation between the positions of the LOSVD peaks, the circular velocity at the shell edge radius v_c , and the shell velocity:

$$v_s^2 = v_c^2(1 - R/r_{s0}) + \frac{v_{los,max+} v_{los,max-}}{4(R/r_{s0})^2(1 + R/r_{s0})^2 - 1}. \quad (22)$$

We substitute the values of $v_{c,slope}$ derived from the “measurements” (that we now know to better describe the real circular velocity of host galaxy) into this relation, thus obtaining the improved “measured” shell velocity $v_{s,eq(22)-slope}$ (see Table 4 and Fig. 15).

In the zone between the current turning points and the shell edge, the inner peaks coalesce and gradually disappear (see Fig. 4). The simulated data do not show such an abrupt and clear disappearance of the inner peaks as the theoretical LOSVD profiles predict, thus even in this zone, we can usually “measure” one inner peak at 0 km/s. The information from these “measurements” is degenerate, and therefore we defined a subsample of simulated “measurements” that includes only those with four clear peaks in the LOSVD (in the columns labeled with SS in Tables 3 and 4).

The spread of the values derived using the approximative maximal LOS velocities–Eqs. (18) and (19) is significantly lower for the subsample ($v_{c,eq(19)}^{SS}$ and $v_{s,eq(18)}^{SS}$) due to the exclusion of areas where these equations do not hold well. On the contrary, the slope of the linear regression in Eq. (21) using the slope of the LOSVD intensity maxima gives a worse result (with a larger error) for the subsample $v_{c,slope}^{SS}$.

The third option to derive the circular velocity v_c at the shell edge radius r_s and shell velocity v_s from the simulated data is to use the approximative LOSVD–Eq. (15), which corresponds to the model shown in purple lines in pictures throughout the text (see Sect. 5, point 2). However, this requires a numerical solution of the equation for a given pair of v_c and v_s . We minimized

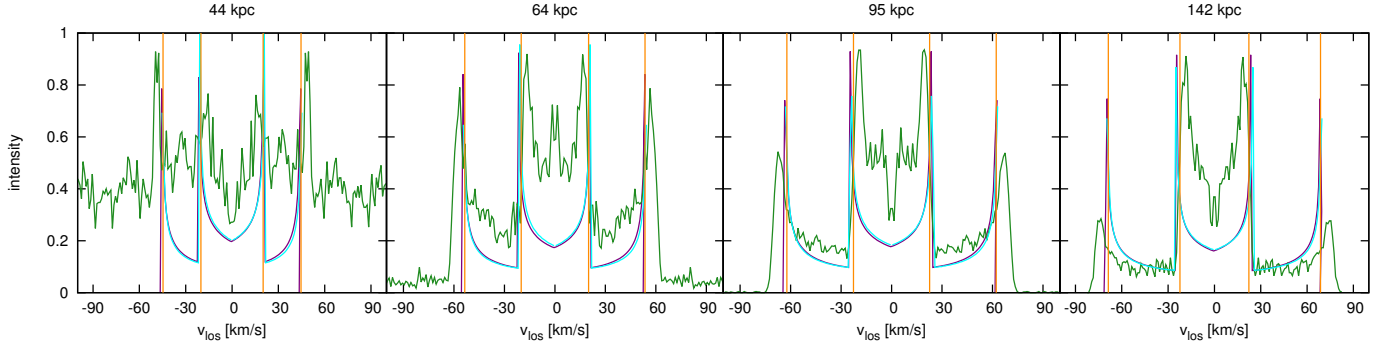


Fig. 12. LOSVDs of four shells at projected radii $0.9r_s$ (indicated as the title of each plot) 2.2 Gyr after the decay of the cannibalized galaxy (parameters of the shells are shown in Table 2). The simulated data are shown in green, the LOSVDs according to the approximative LOSVD (see Sect. 5, point 2) – Eq. (15) in purple, and those according to the model of radial oscillations (Sect. 2.3) in light blue. The graph also shows the locations of the peaks using the approximative maximal LOS velocities (see Sect. 5, point 3) – Eq. (17) – orange lines. Profiles do not include stars of the host galaxy, which are not part of the shell system. The theoretical profiles are scaled so that the intensity of their highest peak approximately agrees with the highest peak of the simulated data. Intensity is given in relative units, so maxima of the profiles have values about 0.9.

Table 3. Circular velocity at the shell edge radius r_s derived from the “measurement” of the simulated data 2.2 Gyr after the decay of the cannibalized galaxy.

r_s kpc	$v_{c,model}$ km/s	N_{data}	N_{data}^{SS}	$v_{c,eq(18)}$ km/s	$v_{c,eq(18)}^{SS}$ km/s	$v_{c,slope}$ km/s	$v_{c,slope}^{SS}$ km/s	$v_{c,fit}$ km/s	$v_{c,slope(MK98)}$ km/s
48.8	326	4	5	346 ± 130	340 ± 94	322 ± 19	314 ± 32	318 ± 51	449 ± 26
–70.6	390	5	7	394 ± 85	390 ± 53	391 ± 5	392 ± 11	368 ± 60	570 ± 23
105.0	441	8	11	478 ± 144	452 ± 64	440 ± 5	447 ± 7	427 ± 28	632 ± 9
–157.8	450	10	15	497 ± 236	472 ± 79	462 ± 8	484 ± 14	460 ± 32	671 ± 11

Notes. r_s and $v_{c,model}$ have the same meaning as in Table 2. N_{data} : number of “measurements” for each shell; $v_{c,eq(18)}$: the mean of values derived from the approximative maximal LOS velocities – Eq. (18) with its mean square deviation; $v_{c,slope}$: a value derived from linear regression using the slope of the LOSVD intensity maxima – Eq. (21) and its standard error (see also Fig. 14); $v_{c,fit}$: a value derived by fitting a pair of v_c and v_s in the approximative LOSVD (Sect. 5, point 2) – Eq. (15), see Fig. 13; $v_{c,slope(MK98)}$: the mean of values derived from the slope of the LOSVD intensity maxima – Eq. (21) with its standard error (see also Fig. 14), but in the equation Δv_{los} is substituted with the distance between the two outer peaks of the LOSVD intensity maxima, in order to mimic the measurement as originally proposed by MK98 for double-peaked profile. The quantities with the superscript SS correspond to the subsample where the “measurements” without two discernible inner peaks in the LOSVD are not used.

Table 4. Velocity of the shell at the radius r_s derived from the “measurement” of the simulated data 2.2 Gyr after the decay of the cannibalized galaxy.

r_s kpc	$v_{s,model}$ km/s	N_{data}	N_{data}^{SS}	$v_{s,sim}$ km/s	$v_{s,eq(19)}$ km/s	$v_{s,eq(19)}^{SS}$ km/s	$v_{s,eq(22)-slope}$ km/s	$v_{s,eq(22)-slope}^{SS}$ km/s	$v_{s,fit}$ km/s
48.8	38.7	4	5	38.7 ± 2.1	50.7 ± 2.3	51.7 ± 1.1	44.2 ± 6.5	44.9 ± 6.3	53.1 ± 2.5
–70.6	54.3	5	7	59.8 ± 1.6	60.8 ± 9.8	65.6 ± 2.0	60.7 ± 10.8	66.0 ± 2.9	66.0 ± 2.6
105.0	63.5	8	11	68.1 ± 1.9	74.8 ± 4.6	76.5 ± 1.4	68.0 ± 8.9	71.3 ± 2.5	78.9 ± 1.0
–157.8	72.4	10	15	74.3 ± 1.2	84.4 ± 5.4	86.7 ± 2.0	78.7 ± 10.5	$82. \pm 3.5$	85.4 ± 2.0

Notes. r_s , $v_{s,model}$, and $v_{s,sim}$ have the same meaning as in Table 2. N_{data} : number of “measurements” for each shell; $v_{s,eq(19)}$: the mean of values derived from the approximative maximal LOS velocities – Eq. (19) with its mean square deviation; $v_{s,eq(22)-slope}$: the mean of values derived from the hybrid relation – Eq. (22) with its mean square deviation (see also Fig. 15); $v_{s,fit}$: a value derived by fitting a pair of v_c and v_s in the approximative LOSVD (Sect. 5, point 2) – Eq. (15), see Fig. 13. The quantities with the superscript SS correspond to the subsample where the “measurements” without two discernible inner peaks in the LOSVD are not used.

the sum of sums of squared differences between $v_{los,max\pm}(v_c, v_s)$ as given by the approximative LOSVD and the simulated data, to obtain best fitted values $v_{c,fit}$ and $v_{s,fit}$. See Tables 3 and 4 for the results. Errors were estimated using the ordinary least squared minimization as if each function $v_{los,max\pm}(v_{c,fit}, v_{s,fit})$ and $v_{los,max\pm}(v_{c,fit}, v_{s,fit})$ was fitted separately – quoted is the larger of the two errors. The LOSVD intensity maxima resulting from this procedure are plotted in Fig. 13 together with the fitted data and the maxima given by the model of radial oscillations (Sect. 2.3).

For the sake of comparison with the method of MK98 we calculated the circular velocity $v_{c,slope(MK98)}$ at the shell edge

radius r_s using the slope of the LOSVD intensity maxima – Eq. (21), where we assume Δv_{los} to be the distance between the two outer peaks of the LOSVD intensity maxima to mimic the measurement of the circular velocity according to the equation (7) in MK98, which was derived for the double-peaked profile. In Table 3 and Fig. 14, we can easily see that these values $v_{c,slope(MK98)}$ differ from the actual circular velocity of the host galaxy $v_{c,model}$ by a factor of 1.3–1.5.

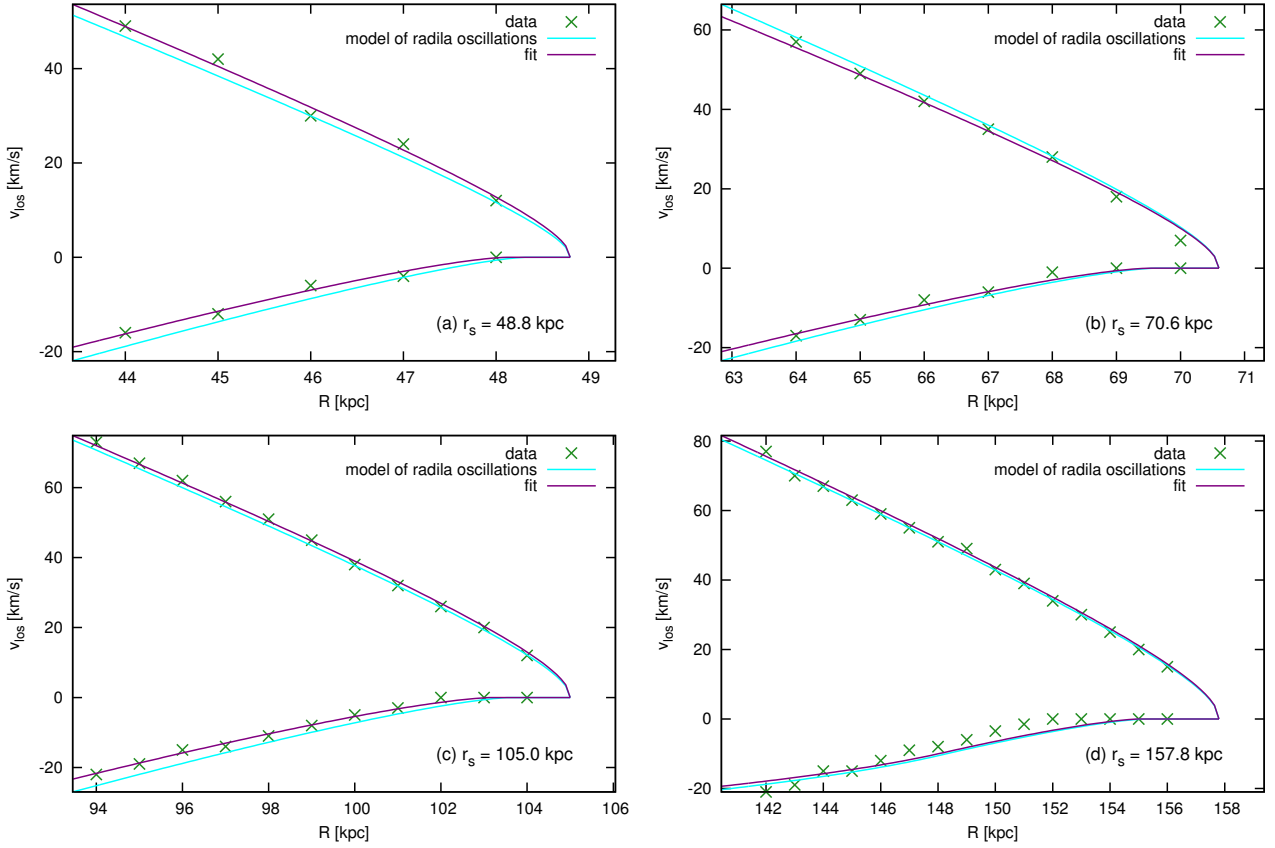


Fig. 13. Fits for the circular velocity v_c and shell velocity v_s using the approximate LOSVD (see Sect. 5, point 2) – Eq. (15) for four shells (r_s indicated in bottom right corner of each plot) in the simulation 2.2 Gyr after the decay of the cannibalized galaxy. The best fit is the purple curve and its parameters are shown in Tables 3 and 4 in the columns labeled $v_{c,\text{fit}}$ and $v_{s,\text{fit}}$. The green crosses mark the “measured” maxima in the LOSVD and the light blue curves show the locations of the theoretical maxima derived from the host galaxy potential according to the model of radial oscillations (see Sect. 2.3). Note that the values of v_c and v_s used in the approximative LOSVD for the purple line were obtained by fitting of the parameters to the simulated data, whereas in Figs. 7, 8, and 12 the values are known from the model of the host galaxy potential.

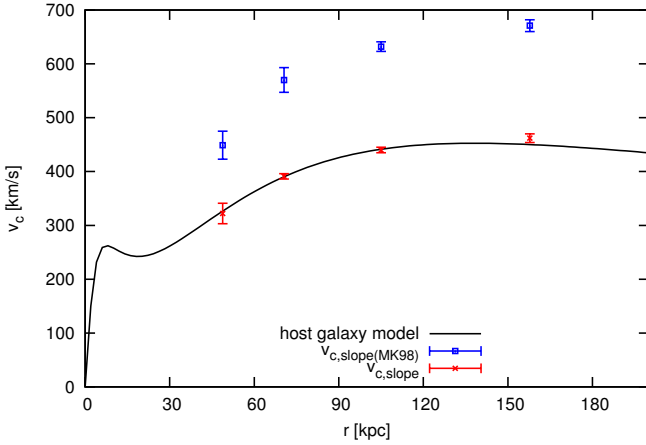


Fig. 14. Circular velocity of the model and values derived from the simulated data: $v_{c,\text{model}}$ of the host galaxy model is shown by black line; blue and red points show values of circular velocity as they result from the analysis of the simulated LOSVD, see Sect. 6.2 and Table 3 for the numbers.

6.4. Instrumental LOSVD

When observed, the LOSVD is always influenced by the instrumental dispersion, which naturally smoothes features of the spectral profile. In Fig. 16, we show the LOSVDs from the sim-

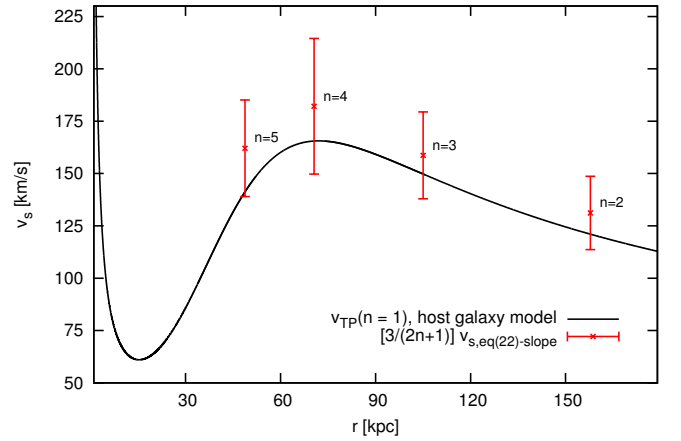


Fig. 15. Comparison of velocity of the shell as a function of radius from the model and the simulated data. Velocity for the first shell ($n = 1$) in the host galaxy model is shown by the black line. Red crosses show $v_{s,\text{eq}(22)\text{-slope}}$ (see Table 4) as they result from the analysis of the simulated LOSVD. Values are corrected for shell number n by the factor $3/(2n + 1)$ so they correspond to velocity of the first shell (see e.g., Eq. (3)).

ulated data smoothed with different Gaussians representing the instrumental profiles having the FWHM 10, 30, and 60 km/s. It

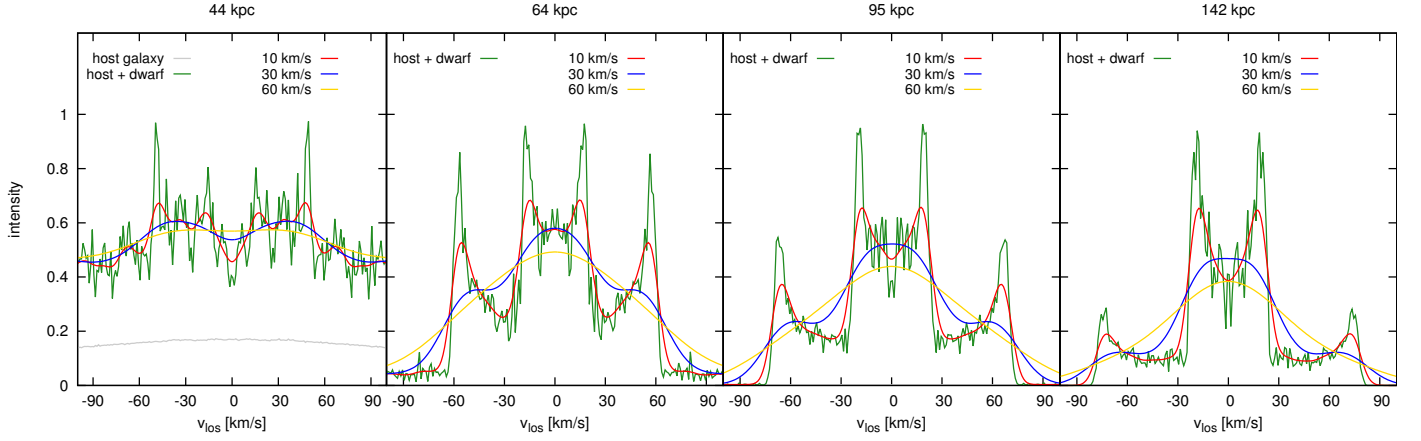


Fig. 16. Line profiles of four shells at projected radii $0.9r_s$ (indicated as the title of each plot, same as in Fig. 12) 2.2 Gyr after the decay of the cannibalized galaxy: gray lines show the LOSVDs for the host galaxy at a given radius (except for the radius of 44 kpc the signal of the host galaxy is negligible comparing to the signal from the cannibalized galaxy); green lines show the total LOSVDs from the host and the cannibalized galaxy together; red, blue, and yellow lines show convolutions of the total simulated data with different Gaussians representing the instrumental profiles having the FWHM 10, 30, and 60 km/s, respectively. Scaling is relative, similar as in Fig. 12.

is obvious that relatively high spectral resolution is necessary for observing an imprint of shell peaks in the line profiles.

7. Discussion

We developed a new method to measure the potential of shell galaxies from kinematical data, extending the work of MK98. The method splits into three different analytical and semi-analytical approaches to obtain the circular velocity in the host galaxy, v_c , and the current shell phase velocity, v_s :

1. The approximative LOSVD – using Eq. (15) and an assumption of the behavior of the shell brightness as a function of the shell radius, see Sect. 4.2
2. The approximative maximal LOS velocities – Eqs. (18) and (19), see Sect. 4.4
3. Using the slope of the LOSVD intensity maxima in the $R - v_{\text{los}}$ diagram – Eq. (21), see Sect. 4.4

In Sect. 5, the first two approaches are compared to the model of radial oscillations (numerical integration of radial trajectories of stars in the host galaxy potential, see Sect. 2). All three approaches are then applied to data for the four shells obtained from a test-particle simulation and compared to the theoretical values, see Sect. 6.2.

Using approach 1. requires a numerical solution of Eq. (15) and the search of a pair of v_c and v_s , which matches the (simulated) data the best. Although this approach is not limited by any assumptions about the radius of the maximal LOS velocity (see Sect. 4.3), it does not give a better estimate of v_c and v_s for our simulated shell galaxy than the other two methods. The deviation from the real value of v_c is between 2 % and 6 %.

Approach 2., using the approximative maximal LOS velocities, results in simple analytical relations and is the only one that can in principle be used for an LOSVD measured at only one projected radius. Nevertheless, when measuring in the zone between the radius of the current turning points and the shell radius, we can expect very bad estimates of v_c and v_s . The mean value from more “measurements” of the LOSVD peaks for each shell of our simulated shell galaxy has a similar accuracy as the values from approach 1., provided that we include only the

“measurements” outside the zone between the radius of the current turning points and the shell radius.

The best method to derive the circular velocity in the potential of the host galaxy seems to be using the slope of the LOSVD intensity maxima, with a typical deviation in the order of units of km/s when fitting a linear function over all the “measured” positions of the LOSVD peaks for each shell. This circular velocity is then used in the hybrid relation, Eq. (22), to obtain the best estimate of the shell velocity.

All the approaches, however, derive the shell velocity systematically larger than the prediction of the model of radial oscillations $v_{s,\text{model}}$ and the value derived from positions between the times 2.49–2.51 Gyr in the simulation $v_{s,\text{sim}}$, see Table 3. It is because the simulated LOSVD peaks always lie too far out (for the outer peaks) or in (for the inner peaks) when compared to the model of radial oscillations. That can be caused by non-radial trajectories of the stars of the cannibalized galaxy, or by the fact that the shell radius in the simulation is poorly defined.

Nevertheless, the shell velocity depends – even in the simplified model of an instant decay of the cannibalized galaxy in a spherically symmetric host galaxy (see Sec. 2) – on the serial number of the shell n and on the whole potential from the center of the galaxy up to the shell radius (see Eq. (3)). The comparison of its measured velocity to theoretical predictions is possible only for a given model of the potential of the host galaxy and the presumed serial number of the observed shells. In such a case it can, however, be used to exclude some parameters or models of the potential that would otherwise fit the observed circular velocity.

The first shell has a serial number equal to one. A higher serial number means a younger shell. On the same radius, the velocity of each shell is always smaller than that of the previous one. In practice, it is of course difficult to establish whether the outermost observed shell is the first created, or whether the first shell (or even the first couple of shells) are already unobservable. Here we can use the potential derived from our (or completely different) method in a reverse way – to determine the velocity of the first shell on the given radius and to compare it to the velocity derived from the positions of the LOSVD peaks. Knowing the serial number of the outermost shell and its position allows us then to determine the time from the merger and the impact di-

rection of the cannibalized galaxy. Moreover, the measurement of shell velocities reveals the presence of shells from different generations (Bartořkov et al. 2011).

The presented method to measure the potential of shell galaxies has several limitations. Theoretical analyses were conducted over spherically symmetric shells and the test-particle simulation was run for a strictly radial merger and analyzed in a projection plane parallel to the axis of the merger. Moreover, both the analytical analysis and the simulations assume spherical symmetry of the potential of the host galaxy. In reality, the regular shell systems with more shells in one galaxy are more often connected to galaxies with significant ellipticity (Dupraz & Combes 1986). Moreover, in cosmological simulations with cold dark matter, halos of galaxies are described as triaxial ellipsoids (e.g., Jing & Suto 2002; Bailin & Steinmetz 2005; Allgood et al. 2006). However, the effect of the ellipticity of the isophotes of the host galaxy on the shell kinematics need not be dramatic, as the shells have the tendency to follow equipotentials that are in general less elliptical than the isophotes. Dupraz & Combes (1986) concluded that the ellipticity of observed shells themselves is in general low, but neatly correlated to the eccentricity of the host galaxy. Prieur (1988) pointed out that the shells in NGC 3923 are much rounder than the underlying galaxy and have an ellipticity which is similar to the inferred equipotential surfaces. This idea was originally put forward by Dupraz & Combes (1986) who found such a relationship for their merger simulations. Furthermore, our method is in principle applicable even to shells spread around the galactic center that are usually connected to more round elliptical galaxies if they were created in a close-to-radial merger. Nevertheless, the combination of the effects of the projection plane, merger axis, and ellipticity of the host galaxy can modify our results and require further analyses.

Because the kinematics of the stars that have once left the cannibalized galaxy is in principle a test-particle problem, it should not be much affected by self-gravity of the cannibalized galaxy and the dynamical friction that this galaxy undergoes during the merger, both of which have been neglected in this work.

Another complication is that the spectral resolution required to distinguish all four peaks is probably quite high (see Sect. 6.4 and Fig. 16) and the shell contrast is usually small. Nevertheless there is the possibility to measure shell kinematics using the LOS velocities of individual globular clusters, planetary nebulae, and, in the Local group of galaxies, even of individual stars.

8. Conclusions

Kinematics of regular shells produced during nearly radial minor mergers of galaxies can be used to constrain their gravitational force field and thus the dark matter distribution. Merrifield & Kuijken (1998) showed that the line-of-sight velocity distribution measured near the edges of a shell has a double-peaked shape, and found a relation between the values of the two LOS velocity peaks and the circular velocity. Their approximation is limited to stationary shells.

We have extended their theoretical analysis to traveling shells. We find that in two-component giant galaxies with realistically massive dark matter halos, the shell propagation velocity is significantly higher, typically 30–150 km/s, compared to values quoted in the theoretical studies in the literature. We show that such large speeds have considerable impact on the LOS kinematics of shells. We show that each peak of the double-peaked profile is split into two, producing a quadruple-peaked LOSVD. We derive a new approximation, relating the circular velocity of the host galaxy potential at the shell edge radius, as

well as the current phase velocity of the shell, to the positions of the four peaks.

In galaxies with multiple shells, we can use circular velocities measured by these methods to determine the potential of the host galaxy over a large span in radii, whereas the measured shell phase velocity carries information on the age of the shell system, and the arrival direction of the cannibalized galaxy. The potential observation of multi-generation shell systems further contains additional limits on the shape of the potential of the host galaxy.

Acknowledgements. We acknowledge support from the following sources: grant No. 205/08/H005 by Czech Science Foundation (IE, LJ, MK, KB, and TS); grant MUNI/A/0968/2009 by Masaryk University in Brno (LJ, KB, and TS); research plan AV0Z10030501 by Academy of Sciences of the Czech Republic (IE, BJ, MK, MB, KB, and IS); grant LC06014 – Center for Theoretical Astrophysics – by Czech Ministry of Education (BJ and IS); and the project SVV261301 by Charles University in Prague (IE, MK, and MB). This work has been done with the support for a long-term development of the research institution RVO67985815 (IE, BJ, MB, and KB). LJ acknowledges the support by the 2-years ESO PhD studentship, held in ESO, Santiago.

References

- Allgood, B., Flores, R. A., Primack, J. R., et al. 2006, *MNRAS*, 367, 1781
- Arp, H. 1966, *ApJS*, 14, 1
- Auger, M. W., Treu, T., Bolton, A. S., et al. 2010, *ApJ*, 724, 511
- Bailin, J. & Steinmetz, M. 2005, *ApJ*, 627, 647
- Balcells, M. & Sancisi, R. 1996, *AJ*, 111, 1053
- Bartořkov, K., Jungwiert, B., Ebrov, I., Jlkov, L., & Křzek, M. 2011, *Simulations of Shell Galaxies with GADGET-2: Multi-Generation Shell Systems*, ed. I. Ferreras & A. Pasquali, 195
- Canalizo, G., Bennert, N., Jungwiert, B., et al. 2007, *ApJ*, 669, 801
- Charmandaris, V., Combes, F., & van der Hulst, J. M. 2000, *A&A*, 356, L1
- Churazov, E., Forman, W., Vikhlinin, A., et al. 2008, *MNRAS*, 388, 1062
- Churazov, E., Tremaine, S., Forman, W., et al. 2010, *MNRAS*, 404, 1165
- Coccato, L., Gerhard, O., Arnaboldi, M., et al. 2009, *MNRAS*, 394, 1249
- Colbert, J. W., Mulchaey, J. S., & Zabludoff, A. I. 2001, *AJ*, 121, 808
- Coleman, M., Da Costa, G. S., Bland-Hawthorn, J., et al. 2004, *AJ*, 127, 832
- Das, P., Gerhard, O., Churazov, E., & Zhuravleva, I. 2010, *MNRAS*, 409, 1362
- de Lorenzi, F., Gerhard, O., Coccato, L., et al. 2009, *MNRAS*, 395, 76
- Deason, A. J., Belokurov, V., Evans, N. W., & McCarthy, I. G. 2012, *ApJ*, 748, 2
- Duc, P.-A., Cuillandre, J.-C., Serra, P., et al. 2011, *MNRAS*, 417, 863
- Dupraz, C. & Combes, F. 1986, *A&A*, 166, 53
- Dupraz, C. & Combes, F. 1987, *A&A*, 185, L1
- Ebrov, I., Jlkov, L., Jungwiert, B., et al. 2011, *Quadruple-Peaked Line-of-Sight Velocity Distributions in Shell Galaxies*, ed. I. Ferreras & A. Pasquali, 225
- Ebrov, I., Jungwiert, B., Canalizo, G., Bennert, N., & Jlkov, L. 2010, in *Astronomical Society of the Pacific Conference Series*, Vol. 423, *Galaxy Wars: Stellar Populations and Star Formation in Interacting Galaxies*, ed. B. Smith, J. Higdon, S. Higdon, & N. Bastian, 236
- Fardal, M. A., Babul, A., Guhathakurta, P., Gilbert, K. M., & Dodge, C. 2008, *ApJ*, 682, L33
- Fardal, M. A., Guhathakurta, P., Babul, A., & McConnachie, A. W. 2007, *MNRAS*, 380, 15
- Fardal, M. A., Guhathakurta, P., Gilbert, K. M., et al. 2012, *MNRAS*, 3140
- Fukazawa, Y., Botoya-Nonesu, J. G., Pu, J., Ohto, A., & Kawano, N. 2006, *ApJ*, 636, 698
- Gavazzi, R., Treu, T., Rhodes, J. D., et al. 2007, *ApJ*, 667, 176
- Heisler, J. & White, S. D. M. 1990, *MNRAS*, 243, 199
- Helmi, A., Navarro, J. F., Meza, A., Steinmetz, M., & Eke, V. R. 2003, *ApJ*, 592, L25
- Hernquist, L. & Quinn, P. J. 1987a, *ApJ*, 312, 17
- Hernquist, L. & Quinn, P. J. 1987b, *ApJ*, 312, 1
- Hernquist, L. & Quinn, P. J. 1988, *ApJ*, 331, 682
- Hernquist, L. & Spergel, D. N. 1992, *ApJ*, 399, L117
- Horellou, C., Black, J. H., van Gorkom, J. H., et al. 2001, *A&A*, 376, 837
- James, R. A. & Wilkinson, A. 1987, in *IAU Symposium*, Vol. 127, *Structure and Dynamics of Elliptical Galaxies*, ed. P. T. de Zeeuw, 471–+
- Jlkov, L., Jungwiert, B., Křzek, M., et al. 2010, in *Astronomical Society of the Pacific Conference Series*, Vol. 423, *Galaxy Wars: Stellar Populations and Star Formation in Interacting Galaxies*, ed. B. Smith, J. Higdon, S. Higdon, & N. Bastian, 243

- Jing, Y. P. & Suto, Y. 2002, *ApJ*, 574, 538
- Kaviraj, S. 2010, *MNRAS*, 406, 382
- Kim, T., Sheth, K., Hinz, J. L., et al. 2012, *ApJ*, 753, 43
- Krajinovi, D., Emsellem, E., Cappellari, M., et al. 2011, *MNRAS*, 414, 2923
- Malin, D. F. & Carter, D. 1983, *ApJ*, 274, 534
- Mandelbaum, R., Seljak, U., & Hirata, C. M. 2008, *J. Cosmology Astropart. Phys.*, 8, 6
- Marino, A., Iodice, E., Tantal, R., et al. 2009, *A&A*, 508, 1235
- Merrifield, M. R. & Kuijken, K. 1998, *MNRAS*, 297, 1292
- Miskolczi, A., Bomans, D. J., & Dettmar, R.-J. 2011, *A&A*, 536, A66
- Nagino, R. & Matsushita, K. 2009, *A&A*, 501, 157
- Nierenberg, A. M., Auger, M. W., Treu, T., Marshall, P. J., & Fassnacht, C. D. 2011, *ApJ*, 731, 44
- Norris, M. A., Gebhardt, K., Sharples, R. M., et al. 2012, *MNRAS*, 421, 1485
- Nulsen, P. E. J. 1989, *ApJ*, 346, 690
- Petric, A., Schiminovich, D., van Gorkom, J., van der Hulst, J. M., & Weil, M. 1997, in *Bulletin of the American Astronomical Society*, Vol. 29, *Bulletin of the American Astronomical Society*, 1344–+
- Prieur, J.-L. 1988, *ApJ*, 326, 596
- Quinn, P. J. 1984, *ApJ*, 279, 596
- Rampazzo, R., Marino, A., Tantal, R., et al. 2007, *MNRAS*, 381, 245
- Rampazzo, R., Plana, H., Longhetti, M., et al. 2003, *MNRAS*, 343, 819
- Romanowsky, A. J., Strader, J., Brodie, J. P., et al. 2012, *ApJ*, 748, 29
- Sanderson, R. E., Mohayaee, R., & Silk, J. 2012, *MNRAS*, 420, 2445
- Schiminovich, D., van Gorkom, J. H., van der Hulst, J. M., & Kasow, S. 1994, *ApJ*, 423, L101+
- Schiminovich, D., van Gorkom, J. H., van der Hulst, J. M., & Malin, D. F. 1995, *ApJ*, 444, L77
- Schweizer, F. 1983, in *IAU Symposium*, Vol. 100, *Internal Kinematics and Dynamics of Galaxies*, ed. E. Athanassoula, 319–326
- Schweizer, F. & Ford, Jr., W. K. 1985, in *Lecture Notes in Physics*, Berlin Springer Verlag, Vol. 232, *New Aspects of Galaxy Photometry*, ed. J.-L. Nieto, 145–+
- Sikkema, G., Carter, D., Peletier, R. F., et al. 2007, *A&A*, 467, 1011
- Stickel, M., van der Hulst, J. M., van Gorkom, J. H., Schiminovich, D., & Carilli, C. L. 2004, *A&A*, 415, 95
- Thomas, J., Saglia, R. P., Bender, R., et al. 2011, *MNRAS*, 415, 545
- Trinchieri, G., Rampazzo, R., Chiosi, C., et al. 2008, *A&A*, 489, 85
- Weijmans, A.-M., Cappellari, M., Bacon, R., et al. 2009, *MNRAS*, 398, 561
- Weijmans, A.-M., Krajinovi, D., van de Ven, G., et al. 2008, *MNRAS*, 383, 1343